

A COMPARATIVE, STRUCTURE FUNCTION-BASED ANALYSIS OF VELOCITY FIELD FORCING TECHNIQUES

Phares L. Carroll¹ and Guillaume Blanquart²

Department of Mechanical Engineering
 California Institute of Technology
 Pasadena, CA 91125, United States
 plcarroll@caltech.edu¹
 g.blanquart@caltech.edu²

ABSTRACT

Without an energy source, a turbulent velocity field will decay with dynamics dictated by the well-known Karman-Howarth equation. In Direct Numerical Simulation (DNS) studies, turbulent fields are maintained at a state of statistical stationarity (constant Taylor-Reynolds number, Re_λ) by supplying such an energy source. The energy source comes in the form of a velocity field forcing method, which involves the addition of a source term to the momentum equation. This momentum source term manifests also in the Karman-Howarth equation, and has a form determined uniquely by the specific forcing method implemented. To ensure the dynamics obtained from the velocity field-forcing methodology are physically correct, their impact on the behavior of the Karman-Howarth equation has been undertaken and attention has been paid to the functional form of the forcing method-imposed source term appended. Two velocity field forcing methods are considered in this study, Lundgren's linear forcing method (Lundgren (2003)) and Alvelius' spectral forcing method (Alvelius (1999)). It was found that the two disparate forcing techniques produce source terms in the Karman-Howarth equation that behave very similarly at small scales, but diverge at the intermediate and large scales. An important consequence of this is that the velocity fields generated by the two methods exhibit comparable statistical and spectral characteristics at these small scales. The contradictory characteristics of the turbulent fields at the large and intermediate scales can be traced similarly back to the differing behavior of the source terms at these scales and their influence on the governing Karman-Howarth equation.

INTRODUCTION TO VELOCITY FIELD FORCING METHODS

The two most commonly-used methods for preventing turbulent velocity field decay are via spectral forcing in wave-space and linear forcing in real-space. Spectral velocity forcing techniques, of which the Alvelius forcing scheme is just one example, are attractive, as they allow for precise control over the location of energy injection. This injection can be concentrated within a small number of modes lying within a specified waveshell, κ_f , with the modes lying outside this waveshell being unimpacted by the forcing term.

The implementation of Alvelius' spectral forcing

scheme results in a (spectral space) momentum equation of the form shown in Eq. 1, where $\hat{f}(\underline{\kappa}, t)$ is a solenoidal forcing term constructed from geometric constraints and \mathcal{F} denotes the Fourier transform. The forcing term is active only within a narrow band of waveshells, $2 \leq \kappa \leq 4$, and it is defined to be locally mutually orthogonal to the wavevector and to the velocity Fourier vector. This orthogonality prevents the source term, $\hat{f}(\underline{\kappa}, t)$, from being correlated with the velocity field, preventing the velocity field and forcing term from developing any detrimental coupling.

$$\frac{\partial \hat{\mathbf{u}}}{\partial t} = \mathcal{F} \left(\nu \nabla^2 \mathbf{u} - \mathbf{u} \cdot \nabla \mathbf{u} - \nabla \left(\frac{p}{\rho} \right) \right) + \hat{f}(\underline{\kappa}, t) \quad (1)$$

More attractive from an implementation perspective is a physical-space forcing technique. Physical-space techniques can be integrated into non-spectral codes and do not require periodic boundary conditions, a restriction of spectral schemes. Lundgren (2003) developed such a forcing (termed "linear forcing" throughout this paper), which was successfully implemented by Rosales & Meneveau (2005). Lundgren's linear forcing method injects energy into the velocity field in proportion to the magnitude of the velocity field fluctuations, \mathbf{u} . This injection is biased preferentially towards the production scales. As the amplitude of the fluctuations typically scales with length, the larger flow scales are supplied with more energy compared to the smaller flow scales. In this respect, it is consistent with spectral forcing schemes, although the linear scheme acts over all scales of the flow. When implemented, the momentum equation that is derived is shown in Eq. 2, where $Q\mathbf{u}$ is the source term appended and Q is a constant related to the eddy-turnover time of the velocity field, τ .

$$\frac{\partial \mathbf{u}}{\partial t} + \mathbf{u} \cdot \nabla \mathbf{u} = -\nabla \left(\frac{p}{\rho} \right) + \nu \nabla^2 \mathbf{u} + Q\mathbf{u} \quad (2)$$

Generally, the metrics by which a velocity field forcing is evaluated are its single-point statistics, Reynolds stresses, velocity field variances, and scaling in the energy spectrum. However, it is the argument of this paper that these are not sufficient to ensure adequate performance and physical fidelity. Instead, it is the transfer spectrum, velocity structure functions, and velocity correlation functions that are key in evaluating the character of the turbulence produced by forcing techniques.

SIMULATION STUDY

The configuration of interest is triply periodic box turbulence. The turbulence contained within the computational domain is homogeneous and isotropic. Thus, the velocity field forcings briefly described will be evaluated against their ability to reproduce the statistical and physical character of such conditions.

To examine the transfer spectra and structure functions of the velocity fields generated by the two forcing techniques, a simulation study was conducted at a constant $Re_\lambda = 140$ with the accepted spatial resolution of $\kappa_{max}\eta = 1.5$ at $N^3 = 512^3$. The kinematic viscosity was 0.0075 and 0.0028 m^2/s for linear and spectral forcing, respectively. This Re_λ is of comparable magnitude to experimentally attainable Re_λ (e.g. Gagne *et al.* (2004), Mydlarski & Warhaft (2006)). The code package used to conduct the study is discretely energy-conserving and implemented in physical space; additional details can be found in Desjardins *et al.* (2008).

The structure of the turbulence generated by each of the two forcing techniques will be examined. Specifically, the second- and third-order longitudinal structure functions are calculated. These are compared to the theoretical scaling laws derived for the inertial subrange. Then, the transfer spectra are calculated to identify the extent (if any) of scale separation present in the flow field. Using the observations from these steps, the effect of the different forcing methods is explored via investigation of their impact on the Karman-Howarth equation. From this analysis, the reasons for the disparities between the linearly- and spectrally-forced turbulent fields are presented.

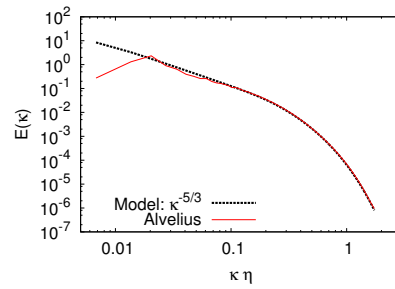
Statistical Behavior

Beginning with single point statistics, the performance of both forcing methods, linear and Alvelius forcing, are comparable. They have been shown to produce the statistical requirements for homogeneous isotropic box turbulence by Alvelius (1999) and Rosales & Meneveau (2005). These requirements were defined to be equal-averaged velocity field variances and zero-averaged Reynolds stresses with reflectional symmetry.

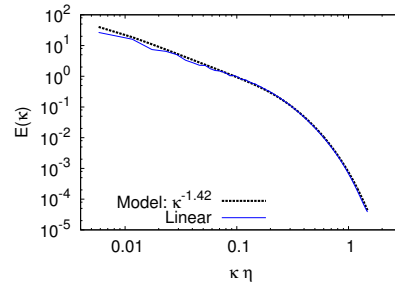
Energy Spectra

The most commonly examined two-point statistic used to qualify the merit of a forcing technique is the resulting energy spectrum, $E(\kappa)$. Specifically, the scaling region across the intermediate wavenumber range is of primary interest. Under sufficiently high Re_λ this region is known as the inertial sub-range, where all dynamics are purely inviscid. Kolmogorov predicted that the energy content within this region ought to scale as $E(\kappa) \sim \kappa^{-5/3}$. Generally, if a forcing scheme is able to reproduce this scaling, it is accepted as valid.

Energy spectra at $Re_\lambda = 140$ are presented in Fig. 1 for both forcing techniques. The energy spectra predicted by these forcing methods are compared to a slightly modified version of the model spectrum offered by Pope (2000), which is defined in Eq. 3. Here, $C(\kappa)$ is a constant of units inverse length, ε is the energy dissipation rate, κ is the wavenumber, L is a large length scale, η is Kolmogorov's scale, and c_η , β , and c_L are constants determined by Re_λ . The model spectrum was used to determine the scaling of the energy spectrum across the inertial subrange, n , by fitting the dissipative region. Upon performing



(a) Alvelius Forcing.



(b) Linear Forcing.

Figure 1. Energy spectra compared to a modified version of the model spectrum defined by Pope (2000) (Eq. 3).

a fit to the DNS-obtained energy spectra, it was determined that the Alvelius-produced spectrum displayed very nearly a $E(\kappa) \sim \kappa^{-5/3}$ scaling across this region, while the linearly-forced spectrum displayed a much weaker scaling with κ , reasonably represented by $E(\kappa) \sim \kappa^{-1.42}$.

$$f_\eta(\kappa\eta) = \exp\left(-\beta\left\{\left((\kappa\eta)^4 + c_\eta^4\right)^{1/4} - c_\eta\right\}\right)$$

$$f_L(\kappa L) = \left(\frac{\kappa L}{\left((\kappa L)^2 + c_L\right)^{1/2}}\right)^{11/3}$$

$$E(\kappa) = C(\kappa)\varepsilon^{2/3}\kappa^{-n}f_L(\kappa L)f_\eta(\kappa\eta) \quad (3)$$

The Alvelius forcing appears to produce an almost perfect $\kappa^{-5/3}$ across the intermediate, supposedly inertial, subrange of wavenumbers. The linear forcing clearly produces a spectrum with a weaker wavenumber scaling. For this reason, among others, spectral forcing is taken generally to be the preferred forcing method for numerical studies of turbulent physics. However, when more closely examined, this is shown to be insufficient to ensure the correct physics and may, in fact, be a misleading metric.

Transfer Spectra

In spectral space, the turbulent kinetic energy equation can be written as Eq. 4, where $E(\kappa, t) = \frac{1}{2}\mathbf{u}(\underline{\kappa}, t) \cdot \mathbf{u}(\underline{\kappa}, t)$ is the turbulent kinetic energy of the fluid, $T(\kappa, t)$ is the energy transfer function, and the last term is viscous energy dissipation at the small scales. This expression mathematically represents the energy transfer (cascade) from the larger scales to the progressively smaller scales. It is the transfer term, $T(\kappa, t)$, which is key in determining the struc-

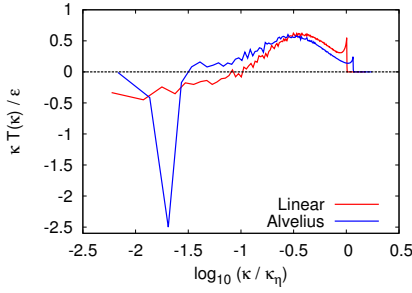


Figure 2. Transfer spectra produced by the two forcing methods. The transfer spectra are averaged over 5 eddy-turnover times. The slight spike near zero is due to simulation resolution. For the present purpose, it can be neglected.

ture of the turbulent field.

$$\frac{\partial E(\kappa, t)}{\partial t} = -\frac{\partial T(\kappa, t)}{\partial \kappa} - 2\nu\kappa^2 E(\kappa, t) \quad (4)$$

For a true inertial sub-range to manifest, there must be complete separation of the production (large, inertial) and the dissipation (small, viscous) scales; no overlap is allowed. Under such conditions, there will be a region of wavenumber space over which the transfer spectrum, $T(\kappa, t)$, will have a value of zero, as rigorously shown by Qian (1997). The true inertial subrange only exists over the region across which $T(\kappa, t) = 0$.

The transfer spectrum for each case in this simulation study was computed according to Eq. 5, and the results are depicted in Fig. 2. The large scales correspond to large negative abscissa values. In Eq. 5, u_i is the pertinent component of velocity, $(\hat{\cdot})$ denotes a Fourier coefficient, $(\cdot)^*$ denotes complex conjugation, and \mathcal{F} denotes the Fourier transform. From Fig. 2, one can note that in neither case is there any discernible wavenumber range over which the value of the transfer spectrum assumes a value of zero. As $Re_\lambda = 140$ is not tremendously high, this is not surprising.

$$T(\kappa, t) = -\hat{u}_i^* \mathcal{F} \left(u_j \frac{\partial u_i}{\partial x_j} \right) \quad (5)$$

If the Re_λ is too low, the anisotropy at the large-scales can penetrate into the smaller scales of the flow. This permeation of anisotropy is known as the finite- Re_λ effect. A consequence of such an effect is a non-zero transfer spectrum and the loss of inviscid behavior across the intermediate wavenumber range. In the absence of a true inertial region, it is quite unexpected to obtain a $\kappa^{-5/3}$ dependence (Fig. 1(a)).

Structure Functions

The second- and third-order longitudinal structure functions are defined in Eq. 6. In Eq. 6, $\langle \cdot \rangle$ denote volumetric spatial averages and r is the distance (magnitude) by which two points in an isotropic flow field (\mathbf{u}) are separated along the direction of unit vector \mathbf{l} . Within the inertial subrange, these structure functions admit known scalings, as provided in Eq. 7 (Lundgren (2002)).

$$\begin{aligned} B_{II}(r, t) &= \langle [\mathbf{u}(\mathbf{x} + r\mathbf{l}, t) - \mathbf{u}(\mathbf{x}, t)]^2 \rangle \\ B_{III}(r, t) &= \langle [\mathbf{u}(\mathbf{x} + r\mathbf{l}, t) - \mathbf{u}(\mathbf{x}, t)]^3 \rangle \end{aligned} \quad (6)$$

$$(a) B_{II}(r, t) \sim C_K(\epsilon r)^{\frac{2}{3}} \quad (b) B_{III}(r, t) \sim -\frac{4}{5}\epsilon r \quad (7)$$

It is from these scalings that the classic $\kappa^{-5/3}$ law for the energy spectrum comes. It has been shown experimentally by Gagne *et al.* (2004) and analytically by Qian (1997) that, for $Re_\lambda < O(10^3)$, B_{II} and B_{III} do not exhibit these asymptotic scalings; there is not sufficient scale separation at these Re_λ to support inviscid dynamics. Moreover, Mydlarski & Warhaft (2006) and Moisy *et al.* (1999) have reported a scaling constant less than $-5/3$ for experimental studies at comparable Re_λ .

The second- and third-order longitudinal structure functions were calculated for both cases included in this study. As depicted in Fig. 3(a) and Fig. 3(b), the asymptotic scaling values indicated in Eq. 7 are not obtained. When compensated, B_{III} is not 0.8 and B_{II} is not $C_K = 2$ across any range of scales. In fact, B_{II} for the spectral forcing exceeds the asymptotic limit of 2, in violation of empirical evidence. However, when examining the energy spectra previously presented in Fig. 1, a discrepancy arises.

Alvelius' spectral forcing, even at the relatively low $Re_\lambda = 140$ (Fig. 1(a)), is exhibiting very near to the Kolmogorov-predicted $\kappa^{-5/3}$ scaling, suggesting the presence of inviscid dynamics in contradiction to the behavior indicated by its structure functions. There is a clear inconsistency present in these spectral scheme results. Meanwhile, the linear forcing does not produce a $\kappa^{-5/3}$, fully consistent with the behavior of its structure functions and with published experimental data. This suggests that there might be a fundamental inconsistency between the spectral forcing technique and the underlying turbulent physics it is trying to reproduce. This is a concerning result, the implications and cause of which will be considered in the following sections.

THE KARMAN-HOWARTH EQUATION

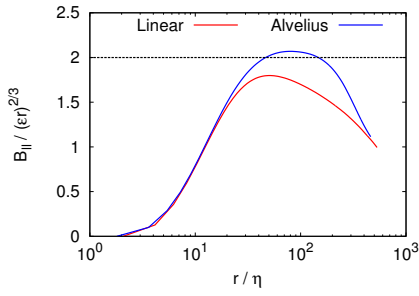
The Karman-Howarth equation relates the evolution of second- and third-order longitudinal structure functions for a decaying, isotropic turbulent field (Landau & Lifshitz (1989), Monin & Yaglom (1975)). In this work, the "forced" Karman-Howarth equation is considered.

The Derivation of the Karman-Howarth Equation

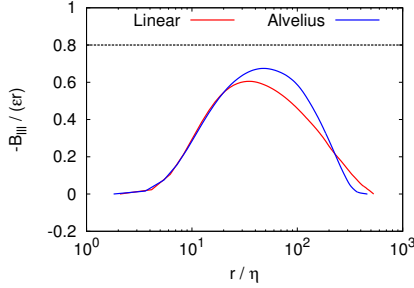
The Karman-Howarth equation is given in Eq. 8, where U^2 is the average velocity field variance. The two terms on the right-hand side represent the inertial (inviscid) processes, through which the energy cascade is able to transfer energy downward, and the dissipation term, through which kinetic energy is dissipated by molecular viscosity. The left-hand side term represents the time rate of change of kinetic energy within the flow itself. Thus, to prevent the decay of turbulence, as is the objective of any simulation forcing scheme (*e.g.* Alvelius' spectral forcing, Lundgren's linear forcing), the scheme implemented must compensate for this left-hand side term.

$$\frac{\partial U^2}{\partial t} - \frac{1}{2} \frac{\partial B_{II}}{\partial t} = \frac{1}{6r^4} \frac{\partial (r^4 B_{III})}{\partial r} - \frac{\nu}{r^4} \frac{\partial}{\partial r} \left(r^4 \frac{\partial B_{II}}{\partial r} \right) \quad (8)$$

The specific form of the left-hand side time derivative is contingent upon the condition of isotropy. As discussed by Monin & Yaglom (1975), the following equality



(a) Second-order longitudinal structure functions.



(b) Third-order longitudinal structure functions.

Figure 3. Structure functions produced by the two forcing methods. Accepted asymptotic limits are indicated by dashed lines. Structure functions are reported for half of the computational domain, $r = [0, \pi]$, and are compensated.

has been applied: $B_{||}(r,t) = 2 [D_{||}(0,t) - D_{||}(r,t)]$, where $D_{||}(r,t) = \langle u_l(\mathbf{x},t)u_l(\mathbf{x} + r\mathbf{1},t) \rangle$ is the longitudinal velocity correlation function. Accordingly, the time derivative term can be expressed as Eq. 9. In component form, this time derivative is written as Eq. 10, where $u(\mathbf{x} + r\mathbf{1}) = u'$.

$$\frac{\partial D_{||}(r,t)}{\partial t} = \frac{\partial \langle u_l(\mathbf{x},t)u_l(\mathbf{x} + r\mathbf{1},t) \rangle}{\partial t} = \frac{\partial U^2}{\partial t} - \frac{1}{2} \frac{\partial B_{||}}{\partial t} \quad (9)$$

$$\frac{\partial D_{||}(r,t)}{\partial t} = \langle u_i \frac{\partial u'_i}{\partial t} + u'_i \frac{\partial u_i}{\partial t} \rangle \quad (10)$$

By inspection, the source term needed to prevent the decay of the turbulent field must take the form of Eq. 10. Taking the source term in concert with the Karman-Howarth equation (Eq. 8), the ‘‘forced’’ Karman-Howarth equation can be expressed as Eq. 11.

$$\begin{aligned} \frac{\partial D_{||}(r,t)}{\partial t} &= \frac{\partial U^2}{\partial t} - \frac{1}{2} \frac{\partial B_{||}}{\partial t} = \\ &= \frac{1}{6r^4} \frac{\partial (r^4 B_{|||})}{\partial r} - \frac{\nu}{r^4} \frac{\partial}{\partial r} \left(r^4 \frac{\partial B_{||}}{\partial r} \right) + S_{||}(r,t) \end{aligned} \quad (11)$$

The source term in Eq. 11, $S_{||}(r,t)$, is the source term for the longitudinal correlation function, $D_{||}(r,t)$. Note that $D_{||}(r,t)$ is a function of the norm (magnitude) of the two-point separation vector \mathbf{r} . This should be distinguished from the full, three-dimensional source term, $S(\mathbf{r},t)$, that is determined by the forcing method used and the appropriate volume integral of which yields the longitudinal source term.

$$S_{||}(r,t) = \frac{1}{r^3} \int_0^r r^2 S(\mathbf{r},t) dr \quad (12)$$

Forcing-imposed Source Terms

Lundgren’s linear forcing appends a source term of the form $Q\mathbf{u}$ to the momentum equation. By applying this source term to Eq. 10, recalling the definition of the velocity correlation function, $R_{ij}(\mathbf{r},t) = \langle u_i(\mathbf{x} + \mathbf{r},t)u_j(\mathbf{x},t) \rangle$, and making use of correlation function identities (delineated in Lundgren (2003)), the source term that results is given by Eq. 13. This is the source term the linear forcing method imposes for $D_{||}(r,t)$.

$$S_{||}(r,t) = \frac{2Q}{r^3} \int_0^r r^2 R_{ii}(\mathbf{r},t) dr = Q \left(2U^2 - B_{||}(r,t) \right) \quad (13)$$

Alvelius’ narrow waveband forcing necessarily imposes a different source term for $D_{||}(r,t)$ on the Karman-Howarth equation. In the development of this spectral forcing technique, a discretized approach was taken (Alvelius (1999)). In the analysis to follow, $f_i(\mathbf{x})$ is the real-space forcing function obtained from the random solenoidal spectral forcing term, $\hat{f}(\boldsymbol{\kappa})$, i denotes the component of the random force, and n denotes the time-step. The amount of power injected within the specified waveshell band is determined by $P_1 = \frac{1}{2} \hat{f}_i^m \hat{f}_i^m \Delta t$.

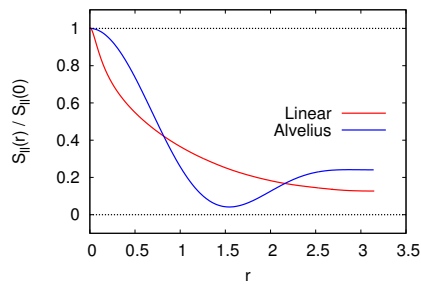
Due to the discrete nature of its derivation, the source term that results is similarly discrete. Writing the time-derivative of velocity as a finite-difference in terms of the real-space analog of $\hat{f}(\boldsymbol{\kappa})$, the source term that is admitted for the Karman-Howarth equation is given in Eq. 14. Here, $\underline{\boldsymbol{\kappa}}$ are those wavevectors which have magnitudes (κ) bounded by $2 \leq \kappa \leq 4$, the power injected is specified to be distributed as a Gaussian centered about $\kappa_f = 3$, and the constants, $C (= 0.5)$ and D , determine the width and correct normalization of the Gaussian, respectively.

$$S(\mathbf{r},t) = \frac{P_1}{2\pi} \sum_{\underline{\boldsymbol{\kappa}}} \frac{\exp(-i\underline{\boldsymbol{\kappa}} \cdot \mathbf{r})}{\kappa^2 \sqrt{D\pi}} \exp\left(-\frac{(\kappa - \kappa_f)^2}{C}\right) \quad (14)$$

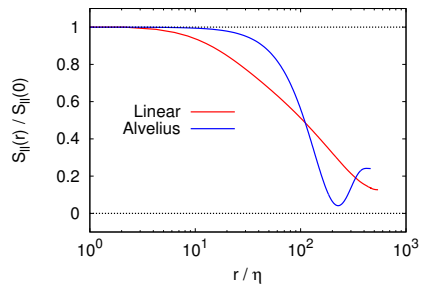
The fact that the linear forcing produces a source term composed of physically-meaningful parameters, while Alvelius’s forcing does not is not surprising. Lundgren proposed a forcing term ($Q\mathbf{u}$) that mimicked the actual mechanism that leads to and sustains naturally occurring turbulent flows, namely shear. Alternatively, Alvelius focused on capturing the statistical nature of turbulence. By creating a solenoidal forcing active only over a contrived region of wavespace, Alvelius ensured the perfect statistical nature of the resulting turbulent velocity fields, although the narrow waveband energy injection employed is not entirely consistent with the physics of a real turbulent flow.

Source Term Behavior

By observation of Fig. 3(a) and Fig. 3(b), the velocity fields produced by these two forcing methods are largely similar at small scales (small r , large κ) and very different at large scales (large r , small κ). Analyzing the functional dependency of their respective source terms on scale size can provide insight into these observations. To facilitate a comparison, the source terms for the longitudinal velocity correlation functions, $S_{||}(r,t)$, for the two forcing methods are evaluated. The results are depicted in Fig. 4. The source terms presented both take the form of autocorrelation functions. This is explicitly stated in Eq. 13 and Eq. 14. It is expected that there is high velocity component correlation at



(a) Large r evolution of $S_{II}(r,t)$



(b) Small r evolution of $S_{II}(r,t)$

Figure 4. Forcing method-imposed source terms appended to the Karman-Howarth equation. One-half of the computational domain is plotted, $r = [0, \pi]$.

small displacements, which becomes progressively weaker as the separation increases. This is what is observed with linear forcing, but not what is present with Alvelius' spectral forcing. With Alvelius' forcing, the increase in correlation of the source term at large separation is due to the injection of energy at these large scales, while the steady, consistent decline in correlation prior is due to the finite bandwidth over which momentum is supplied to the velocity field.

The analysis to follow is broken down into three parts. First, the forced Karman-Howarth equation will be briefly revisited. Second, the small scale source term behavior is investigated. Third, source term behavior at large and intermediate scales is discussed.

Forcing-imposed Correlation Functions

In the forced Karman-Howarth equation (Eq. 11), recall that the time derivative term is equivalent to the time derivative of the longitudinal velocity correlation function, D_{II} . This implies that the effect of velocity field forcing methods is to enforce on the turbulence a prescribed velocity field distribution via a frozen (temporally fixed) longitudinal velocity correlation. The correlation functions calculated from the velocity fields produced by the two forcing methods are illustrated in Fig. 5. By inspection, these curves are in agreement at the small scales ($r/\eta < 30$) and deviate past this point (intermediate and large scales). This suggests that the two forcing methods have the same effect on the turbulence at these small scales, $r/\eta < 30$. It is the source terms that are responsible for prescribing the correlation function on the turbulent field. Thus, the consistency of $D_{II}(r)$ at the small scales and the divergent large scale behavior should be justifiable by examination of the source terms themselves. As an aside, it is noteworthy that $r/\eta \sim 30$ is often considered to be the peak of the dissipation spectrum (Pope

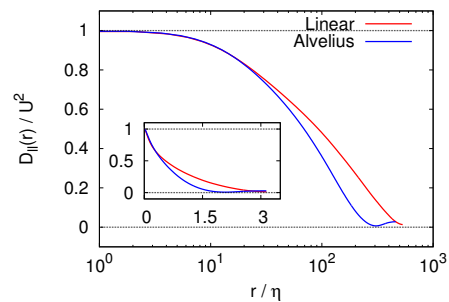


Figure 5. Forcing method-imposed velocity correlation functions. One-half of the computational domain is plotted, $r = [0, \pi]$. Inset shows r vs. $D_{II}(r)/U^2$.

(2000)).

Dissipation Range Restricting attention to the small scales, in the limit of $r \rightarrow 0$ under stationary conditions, the forced Karman-Howarth equation will retain only the applied source term and the viscous term, as $B_{III}(r)$ can be expected to be negligible in this viscosity-dominated region. As it has been shown that the two source terms behave quite similarly in this small scale region, both source terms can be represented by Eq. 13. The resulting partial differential equation can be solved for $B_{II}(r)$ via a series solution of the form of Eq. 15. Due to the even nature of the second-order structure function, only even powers of r are needed. Additionally, the definition of $B_{II}(r)$ mandates that the first coefficient term obey $a_0 = 0$, making the leading order term in the expansion parabolic with coefficient $a_1 = \frac{1}{5}QU^2/\nu$.

$$B_{II}(r) = \sum_{n=1}^{\infty} a_n r^{2n} = a_1 r^2 + a_2 r^4 + a_3 r^6 + \dots \quad (15)$$

In the description of the linear forcing method, it was stated that the forcing coefficient, Q , was related to the eddy-turnover time for the velocity field; more exactly, $Q = (2\tau)^{-1}$, where $\tau = k/\varepsilon$, the ratio of turbulent kinetic energy to the viscous dissipation rate. Thus, Q can be written as $Q = \varepsilon/3U^2$. Also, under the condition of isotropy, the dissipation rate can be expressed as $\varepsilon = 15\nu U^2/\lambda_g^2$, where λ_g is the transverse Taylor micro-scale. In light of these expressions, the significance of a_1 becomes clear. In terms of these physical parameters, it can be written $a_1 = \varepsilon/15\nu = U^2\lambda_g^{-2}$, which is the inverse timescale (squared) appropriate for small scale physics. This finding is important, as it suggests that the small turbulent length scales are not affected detrimentally by either of the forcing techniques. Instead, the effect is simply to enforce the physically-appropriate length- and time-scales.

When this series solution for $B_{II}(r)$ was compared to the DNS data for both forcing methods (Fig. 3), agreement was found to persist until approximately $r/\eta \sim 10$, when the viscous effects presumably cease to be dominant. This suggests that past $r/\eta \sim 10$, $B_{III}(r)$ can no longer be neglected and the inertial term begins to manifest. In the comparison, only four terms were included in the series solution; the higher order contributions had negligible impact.

Further, when isolated, the source terms for both forcings assume a value of $S_{II}(r=0) = \frac{2}{3}\varepsilon$ at zero separation. By inspection of the time derivative in the forced Karman-

August 28 - 30, 2013 Poitiers, France

Howarth equation, Eq. 11, at $r = 0$, the second-order structure function necessarily vanishes, leaving only the time-derivative of the velocity field variance, $\frac{\partial U^2}{\partial t}$. This can be confirmed straightforwardly to be equivalent to $\frac{2}{3}\varepsilon$. This finding is key in supporting the claim that the sole impact that these forcings are having at the smallest scales is to compensate for physically-relevant losses. This is additional evidence that at the smallest scales, the forcing methods are not altering artificially the governing physics.

Intermediate and Large Scales One of the objectives of this research was to show that simply attaining the right statistical behavior and an approximate $\kappa^{-5/3}$ scaling in the energy spectrum was not sufficient to verify that a forcing method could reproduce the “correct” physics in the velocity field. Instead, the transfer spectrum, structure functions, and velocity correlation functions are necessary. It has been established in the previous sections that the small scale behavior is captured correctly irrespective of the forcing scheme used, and the metrics calculated there (spectra, structure functions) are consistent with experimental data. However, at the intermediate and large scales, in the case of Alvelius forcing, physical behavior contradictory to experimental data is recovered in both the transfer spectrum and structure function scaling. This suggests that the turbulence at these scales may be suspect in nature, despite the $\kappa^{-5/3}$ scaling obtained in the energy spectrum. This highlights the need to evaluate additional metrics prior to accepting the merit of a velocity forcing method. By determining the behavior of the source term for the correlation function in the governing Karman-Howarth equation, the impact of a forcing technique can be qualified.

Implications for the Karman-Howarth Equation

The behavior of these two source terms have implications for the forced Karman-Howarth equation, which are discussed best in the context of the longitudinal correlation functions the forcing methods impose. The addition of a forcing term to the Karman-Howarth equation freezes in time the velocity correlation function, $D_{ll}(r)$. From observation of Fig. 5, the two forcing methods produce equivalent velocity correlation functions at small r , imposing the same velocity field distribution over these scales. At the intermediate and large scales, however, they are imposing different velocity field correlations (structures) on the turbulence. It is this difference which accounts for their disparity at the larger scales, explains how the two approaches fundamentally impact the behavior of the governing (forced) Karman-Howarth equation, and causes the disagreement between the structure functions, transfer spectra, and energy spectra calculated from the linear and spectral forcing methods.

CONCLUSIONS

In summary, at a $Re_\lambda = 140$, as confirmed by experimental data, there should not be a true inertial subrange of scales. Accordingly, there should not be a $\kappa^{-5/3}$ scaling

region present in the energy spectrum. The linear forcing method produces turbulent physics that are consistent with experimental findings and produces metrics (e.g. structure functions, spectra) that are self-consistent. There is, however, a discrepancy in the velocity field physics produced under the action of Alvelius’ spectral forcing. The energy spectrum does not agree with experimentally obtained scalings for this Re_λ , and it appears to be inconsistent with the transfer spectrum obtained. Additionally, the generated structure functions do not agree with empirical results.

The source terms that each forcing imposes in the Karman-Howarth equation have been investigated. It was found that the source terms display similar behavior at small scales and very different behavior at large scales. These large scale disparities are reflected in the divergent behaviors observed in the energy spectra, transfer spectra, and structure functions calculated. The velocity-field forcing method has been shown to be irrelevant at the small scales, with differences manifesting only outside the dissipation region. Additionally, the differences in the physical character of the turbulence that the two forcing methods produce have been attributed to the differing velocity correlation functions that they impose on the (forced) Karman-Howarth equation.

REFERENCES

- Alvelius, K. 1999 Random forcing of three-dimensional homogeneous turbulence. *Physics of Fluids* **11** (7), 1880.
- Desjardins, O., Blanquart, G., Balarac, G. & Pitsch, H. 2008 High order conservative finite difference scheme for variable density low Mach number turbulent flows. *Journal of Computational Physics* **227** (15), 7125–7159.
- Gagne, Y., Castaing, B., Baudet, C. & Malecot, Y. 2004 Reynolds dependence of third-order velocity structure functions. *Physics of Fluids* **16** (2), 482.
- Landau, L.D. & Lifshitz, E.M. 1989 *Course of Theoretical Physics*, 2nd edn., , vol. 6. Pergamon Press Inc.
- Lundgren, T.S. 2002 Kolmogorov two-thirds law by matched asymptotic expansion. *Physics of Fluids* **14** (2), 638.
- Lundgren, T.S. 2003 Linearly forced isotropic turbulence. *CTR Annual Research Briefs* (2), 461–473.
- Moisy, F., Tabeling, P. & Willaime, H. 1999 Kolmogorov Equation in a Fully Developed Turbulence Experiment. *Physical Review Letters* **82** (20), 3994–3997.
- Monin, A.S. & Yaglom, A.M. 1975 *Statistical Fluid Mechanics: Mechanics of Turbulence*, , vol. 2. The MIT Press.
- Mydlarski, L. & Warhaft, Z. 2006 On the onset of high-Reynolds-number grid-generated wind tunnel turbulence. *Journal of Fluid Mechanics* **320**, 331.
- Pope, S.B. 2000 *Turbulent Flows*. Cambridge University Press.
- Qian, J. 1997 Inertial range and the finite Reynolds number effect of turbulence. *Physical Review E* **55** (1), 337–342.
- Rosales, C. & Meneveau, C. 2005 Linear forcing in numerical simulations of isotropic turbulence: Physical space implementations and convergence properties. *Physics of Fluids* **17** (9), 095106.